ELSEVIER

Dynamics of Atmospheres and Oceans 27 (1997) 549–574

dynamics of atmospheres and oceans

Interaction between the oceanic mesoscale and the surface mixed layer

Dennis J. McGillicuddy Jr. [a,*], Allan R. Robinson [b,1]

[a] *Woods Hole Oceanographic Institution, Woods Hole, MA 02543, USA*
[b] *Department of Earth and Planetary Sciences, Harvard University, Cambridge, MA 02138, USA*

Received 12 January 1996; revised 7 October 1996; accepted 13 November 1996

Abstract

A semianalytic solution to the mutual interaction of a Rossby wave and the surface mixed layer is derived. The presence of the mixed layer causes neither damping nor growth of the interior motions; modal structures and frequencies are simply altered by a small amount. Rossby wave motions perturb the surface boundary layer quite significantly. Vertical transports arising from both the wave itself and its interaction with the Ekman flow cause entrainment and detrainment and create complex remnant layer structures below the mixed layer. The semianalytic solution is used to benchmark a coupled quasigeostrophic and surface boundary layer numerical model. Intricate numerical techniques are required to maintain the fidelity of the mixed layer–remnant layer interface and the structures below it. © 1997 Published by Elsevier Science B.V.

1. Introduction

The upper ocean is a complex and highly dynamic environment which accommodates a tremendous diversity of physical phenomena. In broad terms, variability in the surface boundary layer results from a convoluted mixture of processes arising from three fundamental sources: (1) direct atmospheric forcing, (2) motion in the ocean's interior, and (3) interaction between the previous two. The general characteristics of the oceanic response to local fluxes of heat, salt and momentum through the air–water interface are reasonably well understood (Price et al., 1987); this knowledge has been articulated into a set of one dimensional models which are quite capable of realistically simulating changes in the upper ocean forced directly by the atmosphere (Martin, 1985). Similarly, the structure and variability of mesoscale currents, fronts and eddies has been well

* Corresponding author. Tel.: +1-508-289-2683; fax: +1-508-457-2194.
[1] Tel.: +1-617-495-2819; fax: +1-617-495-5192.

PII S0377-0265(97)00030-4

established (Robinson, 1983). The near surface expressions of these fluctuations in the main thermocline are often times abundantly clear in satellite sea surface temperature imagery, as well as in situ hydrographic observations. In contrast, relatively little is known about how the surface boundary layer and main thermocline mesoscale currents interact.

There has been some exploration of specific aspects of this general topic from a geophysical fluid dynamics point of view. Early theoretical investigations focused on the interaction of steady wind-driven surface currents with specified interior velocity structures. Stern (1965) examined the superposition of Ekman drift on a geostrophic vortex. Niiler (1969) conducted a similar analysis using a jet for the underlying velocity field. Both of these efforts suggested that advection of the interior vorticity by the boundary layer velocity was balanced by relatively intense vertical motion in localized regions within the mesoscale structure. Stevenson (1983) constructed a semianalytic solution for the interaction of Rossby waves with a mixed layer forced by seasonally varying surface fluxes. Lee et al. (1994) used a two dimensional nonhydrostatic primitive equation model to construct comprehensive simulations of the problem originally formulated by Niiler (1969). Diagnosis of the numerical solutions, which contain more complete physics than the original model, shows complex secondary circulations in and around the jet that are set up by its interaction with the wind-driven flow.

Observational inquiry into the interaction problem has in large part emphasized higher frequency phenomena. Weller (1982, 1985) demonstrated that a mesoscale quasigeostrophic deformation field can alter the effective coriolis frequency, thereby modulating inertial oscillations. Kunze (1985) developed a wave–mean flow interaction theory for the propagation of near inertial motions in the presence of geostrophic shear, and presented a mechanism for trapping and amplification of such fluctuations in regions of negative vorticity. The interaction of inertial currents with mesoscale flows was investigated numerically by Klein and Hua (1988), who simulated spatial intermittency in the depth of the mixed layer caused by variations in the local entrainment rate via perturbations in vertical shear brought on by the combination of the inertial motion and interior velocity field.

While it is clear that near inertial motion cannot be neglected in a complete theory of the interaction problem, there are parameter ranges for which their inclusion is not essential. Our aim is to investigate the fundamental mechanisms of this interaction at small Rossby number through examination of a simple idealized case consisting of freely propagating linear Rossby waves in the presence of constant surface forcing. Stevenson (1983) analyzed the mixed layer response to the vertical motions of linear Rossby waves over an annual heating and cooling cycle. His analysis was limited to the effect of the interior motions on the mixed layer itself, with little attention given to the dynamics of the remnant layer below. Here the interaction of the surface boundary layer with linear Rossby waves will be examined in detail over a depth interval that includes both mixed and remnant layers. An approximate analytic solution to the problem will be described for an idealized case. This example is then used as a test case to demonstrate the proper functioning of the three dimensional coupled quasigeostrophic and surface boundary layer numerical model introduced by Walstad and Robinson (1993). This quantitative benchmarking with a semi-analytical solution for an idealized linear (case

validates the numerical model and thus provides a basis for extension of the results into nonlinear regions of parameter space (McGillicuddy et al., 1995; McGillicuddy and Robinson, 1997).

2. Scale analysis

A comprehensive scale analysis of a set of equations governing the interaction of the surface boundary layer with a quasigeostrophic oceanic interior was conducted by Stevenson (1980). [2] For brevity, the results will be presented here in summary form only. The simplest scenario consists of spatially and temporally uniform atmospheric forcing and linear interior motions. In the absence of interior motions, the mixed layer depth is constant and the buoyancy increases linearly with time. The interior motions perturb the mixed layer through their vertical velocities. The mixed layer perturbation consists of a combination of simple displacement of the mixed layer interface and entrainment/detrainment fluxes induced by vertical motions in the interior. Under seasonally varying atmospheric forcing, the situation is somewhat different. When the basic state is detraining and the frequency of the interior motions is much greater than the seasonal frequency, the prior scale analysis still holds. However, for this same class of internal motions, when the basic state is entraining an entirely different balance of terms occurs. Vertical motions of the interior dominate mixed layer fluctuations as the perturbation entrainment rate becomes negligible. Stevenson (1983) examined this particular range of parameter space in an investigation of the seasonally varying interaction between Rossby waves and the mixed layer.

The relative importance of horizontal variations in the basic state is controlled by three nondimensional parameters

$$\lambda = \frac{l}{L} \quad \hat{\omega} = \frac{\omega}{\omega} \quad \delta = \frac{\omega}{f_0}$$

where L is the spatial scale of atmospheric forcing, l and ω are the length and frequency scales of the quasigeostrophic interior motions, Ω is the yearly frequency, and f_0 is the coriolis parameter. For $\lambda \ll \frac{\delta}{\hat{\omega}}$, horizontal advections of the basic state by the interior geostrophic velocity are unimportant. In the range, $\frac{\delta}{\hat{\omega}} \ll \lambda \ll \delta$ horizontal advection of the basic state buoyancy by the interior velocity plays a significant role in determining the perturbation buoyancy in the mixed layer. Nevertheless, it is still the vertical velocities associated with the interior motions that advect the buoyancy below the mixed layer and perturb the mixed layer depth. The full suite of horizontal advection terms become important when $\lambda \gg \delta$. The basic state buoyancy both within and below the mixed layer are advected by the interior velocity. In addition, the mixed layer depth is perturbed by the interior velocity flowing across the bottom of the sloping basic state mixed layer.

Three separate mechanisms by which the ocean's internal motions affect the mixed layer have thus been identified. First, mixed layer buoyancy can be modified by

[2] Contact A.R. Robinson to obtain a copy of the Ph.D. thesis of Stevenson.

horizontal advection by the interior velocity. Second, horizontal interior flow impinging upon a sloping mixed layer bottom can perturb the entrainment rate and the mixed layer depth. Finally, vertical motions caused by the dynamics of the interior and its interaction with the boundary layer flow can cause fluctuations in mixed layer depth and entrainment rate. Of these three potentially important effects only the last will be considered here in an idealized problem corresponding to the simplest scale analysis in which atmospheric forcing is uniform, interior motions are linear, and horizontal variations in the basic state are negligible ($\lambda \ll \frac{\delta}{\tilde{\omega}}$).

3. The model

In order to examine the mutual interaction between the surface boundary layer and linear Rossby waves, a problem is constructed in which the mixed layer depth is constant in the absence of any interior motions (the basic state). This is accomplished by prescribing constant fluxes of momentum and heat through the surface. That is, the wind stirring and heat input through the surface balance to maintain the mixed layer at a fixed depth. First the effect of this mixed layer boundary condition on the linear quasi-geostrophic potential vorticity equation is shown to be small. Thus, the Rossby wave modes can be computed as if the mixed layer were not present. The waves are then used to perturb the basic state mixed layer to permit detailed diagnosis of the interaction between the surface boundary layer and the interior motions. The fundamental connection between the two regimes is a result of vertical motions in their interval of overlap, which arise from two different sources: vortex stretching in the interior and a surface divergence caused by the advection of the interior by the wind driven boundary layer flow. These vertical motions in the upper ocean induce fluctuations in the depth of the mixed layer as well as entrainment and detrainment fluxes through its base, causing the development of complex vertical density structures. A number of numerical techniques are developed to facilitate accurate representation of this solution in the coupled quasigeostrophic and surface boundary layer model.

In this problem, a Kraus–Turner type bulk mixed layer model is used. It is assumed that neither buoyancy nor horizontal velocity vary within the mixed layer. Vertical velocity varies linearly within the mixed layer as a result of the continuity equation and the assumption concerning horizontal velocity. Turbulent diffusion below the mixed layer is not considered in this model, nor is the generation of turbulent kinetic energy due to the shear at the base of the mixed layer. For simplicity it is assumed that all solar radiation is absorbed at the sea surface. The dimensional buoyancy, momentum, turbulent kinetic energy, entrainment and vorticity equations for the mixed layer are

$$h\frac{\partial b}{\partial t} + h\boldsymbol{v}\cdot\nabla b + (b - b_{+})e = B_0 \tag{1a}$$

$$f_0\hat{\mathbf{k}}\times h\boldsymbol{v} = \tau - h(\nabla p)_{-d} \tag{1b}$$

$$\frac{1}{2}h(b - b_{+})e = m_0 u_*^3 - \frac{1}{2}B_0 h - \epsilon_0 h \tag{1c}$$

$$e = \frac{\partial h}{\partial t} + \boldsymbol{v}_+ \cdot \nabla h + w_+ \tag{1d}$$

$$h\frac{\partial \zeta}{\partial t} + f_0 w_+ + \beta h v = \frac{\partial \tau^{(y)}}{\partial x} - \frac{\partial \tau^{(x)}}{\partial y}. \tag{1e}$$

A detailed derivation of these equations is provided in Stevenson (1980). The symbols used in these equations are defined in Table 1.

In order to understand the mutual interaction of the mixed layer and the Rossby waves, the mixed layer quantities ϕ are separated into a basic state $\bar{\phi}$ determined by the atmospheric forcing and a perturbation component caused $\hat{\phi}$ by the Rossby waves ($i.e., \phi = \bar{\phi} + \hat{\phi}$). In this analysis, the mixed layer is forced by a constant wind stress and a constant positive surface buoyancy flux. Therefore, the basic state mixed layer stays at a constant depth and the mixed layer buoyancy increases linearly with time. The basic state equations for buoyancy, momentum and turbulent kinetic energy are

$$\bar{h}\frac{d\bar{b}}{dt} = 1 \tag{2a}$$

$$\hat{\mathbf{k}} \times \bar{h}\bar{\boldsymbol{v}} = \tau \tag{2b}$$

$$1 - \frac{1}{2}\bar{h} - \frac{1}{\hat{B}}\bar{h} = 0 \tag{2c}$$

where $\hat{B} = \frac{B_0}{\epsilon_0}$. Time, mixed layer depth, mixed layer buoyancy, horizontal mixed layer velocity, and wind stress have been scaled as follows:

$$t = wt^*$$

Table 1
Definition of symbols used in the dimensional mixed layer equations

∇	del operator $\left[= \left(\frac{\partial}{\partial x}, \frac{\partial}{\partial y} \right) \right]$
x, y	eastward and northward coordinates
t	time
h	mixed layer depth
b	mixed layer buoyancy
b_+	buoyancy just below the mixed layer
$\mathbf{v}$	vertically averaged horizontal mixed layer velocity $[= (u, v)]$
$\mathbf{v}_+$	horizontal velocity just below the mixed layer
w_+	vertical velocity just below the mixed layer
ζ	mixed layer vorticity $\left[= \left(\frac{\partial v}{\partial x} - \frac{\partial u}{\partial y} \right) \right]$
e	entrainment rate
B_0	surface buoyancy flux
τ	surface wind stress divided by a reference density $[= (\tau^{(x)}, \tau^{(y)})]$
u_*	friction velocity $[= \lvert\tau\rvert^{1/2}]$
p	pressure
d	fixed depth below which there is no direct surface influence
f_0	coriolis parameter
β	northward gradient of the coriolis parameter
m_0	wind generated TKE parameter
ϵ_0	background dissipation
$\hat{\mathbf{k}}$	unit vector in the upward direction

$$\bar{h} = \frac{\bar{h}^*}{\bar{H}}$$

$$\bar{b} = \frac{\bar{b}^*}{\bar{Y}}$$

$$\bar{v} = \frac{\bar{v}^*}{\bar{U}}$$

$$\tau = \frac{\tau^*}{u_*^2}$$

$$\bar{H} = \frac{m_0 u_*^3}{B_0}$$

$$\bar{Y} = \frac{B_0^2}{m_0 u_*^3 w}$$

$$\bar{U} = \frac{B_0}{m_0 u_* f_0}$$

where asterisks indicate dimensional variables and ω is the Rossby wave frequency.

The Rossby waves are governed by the linear quasigeostrophic potential vorticity equation,

$$\frac{\partial \nabla^2 p}{\partial t} + \frac{\partial}{\partial z}\left[\frac{1}{\gamma(z)}\frac{\partial^2 p}{\partial z \partial t}\right] + \frac{\hat{\beta}}{\delta}\frac{\partial p}{\partial x} = 0 \tag{3}$$

where p is the dynamic pressure and $\gamma(z) = S\frac{db_I}{dz}$. The eastward and northward coordinates x and y have been scaled by the horizontal length scale L of the Rossby waves, the vertical coordinate z has been scaled by the depth of the ocean D and the dynamic pressure p has been scaled by $f_0 U_I L$, where U_I is the horizontal velocity scale of the interior motions. The nondimensional numbers are

$$\hat{\beta} = \frac{\beta L}{f_0}$$

$$\delta = \frac{w}{f_0}$$

$$S = \frac{N^2 D^2}{f_0^2 L^2}$$

where N is the Brunt–Väisälä frequency scale for $\frac{db_I^*}{dz^*}$ and $b_I^*(z^*)$ is the vertical structure of buoyancy in the absence of any interior motions.

The interaction between the mixed layer and the Rossby waves is governed by the perturbation buoyancy, horizontal momentum, turbulent kinetic energy, entrainment, vorticity, and buoyancy below the mixed layer (b_r) equations:

$$\bar{h}\frac{\partial \hat{b}}{\partial t} + \hat{h}\frac{d\bar{b}}{dt} + \frac{\overline{Ro}}{\delta}\bar{h}\bar{v}\cdot\nabla\hat{b} + \left(\bar{b} - \bar{b}_+\right)\hat{e} + Ro_I\left(\hat{b} - \hat{b}_+\right)\hat{e} = 0 \tag{4a}$$

$$\hat{\mathbf{k}} \times \bar{h}\hat{\boldsymbol{v}} = -\bar{h}(\nabla p)_{-\bar{h}} \tag{4b}$$

$$\frac{1}{2}\bar{h}\left(\bar{b} - \bar{b}_+\right)\hat{e} + \frac{Ro_I}{2}\bar{h}\left(\hat{b} - \hat{b}_+\right)\hat{e} = -\frac{1}{2}\hat{h} - \frac{1}{\hat{B}}\hat{h} \tag{4c}$$

$$\hat{e} = \frac{\partial \hat{h}}{\partial t} + \frac{\bar{Ro}}{\delta}\bar{\boldsymbol{v}}_+ \cdot \nabla \hat{h} + \hat{w}_+ \tag{4d}$$

$$\bar{h}\frac{\partial \hat{\zeta}}{\partial t} + \frac{\bar{Ro}}{\delta}\bar{h}\bar{\boldsymbol{v}} \cdot \nabla\hat{\zeta} + \hat{w}_+ + \frac{\hat{\beta}}{\delta}\bar{h}\hat{v} = 0 \tag{4e}$$

$$\frac{\partial \hat{b}_r}{\partial t} + \frac{\bar{Ro}}{\delta}\bar{\boldsymbol{v}} \cdot \nabla \hat{b}_r + \hat{w}\frac{d\bar{b}_r}{dz} + \hat{w}\frac{\partial \hat{b}_r}{\partial z} = 0 \tag{4f}$$

The perturbation variables have been scaled as follows:

$$\hat{h} = \frac{\hat{h}^*}{\bar{H}Ro_I}$$

$$\left(\hat{b}, \hat{b}_+\right) = \frac{\left(\hat{b}^*, \hat{b}_+^*\right)}{\bar{Y}Ro_I}$$

$$\hat{b}_r = \frac{\hat{b}_r^*}{\bar{Y}}$$

$$\hat{e} = \frac{\hat{e}^*}{\hat{H}\omega Ro_I}$$

$$\hat{\boldsymbol{v}} = \frac{\hat{\boldsymbol{v}}^*}{U_I}$$

$$\hat{\zeta} = \frac{\hat{\zeta}^*}{U_I/L}$$

$$\left(\hat{w}, \hat{w}_+\right) = \frac{\left(\hat{w}^*, \hat{w}_+^*\right)}{\bar{H}\omega Ro_I}$$

where the Rossby numbers for the interior and boundary layer motions are $Ro_I = \frac{U_I}{f_0 L}$ and $\bar{Ro} = \frac{\bar{U}}{f_0 L}$ respectively. In these perturbation equations many small terms have been neglected. See Stevenson (1980) for a formal scale analysis. Because linear Rossby waves are considered (i.e., $Ro_I \ll \sigma$), all terms of order $\frac{Ro_I}{\delta}$ are neglected.

4. Results

4.1. Linear Rossby wave modes in the presence of a surface mixed layer

In the absence of any forcing, the linear quasigeostrophic potential vorticity equation is an eigenvalue problem. For a horizontally unbounded domain with no boundary layers the solutions to the vorticity equation are freely propagating undamped Rossby wave

modes. In this section, the effect of the surface mixed layer on these linear Rossby wave modes is calculated. It is found that the effect is one of neither damping nor growth.

The surface mixed layer, which is forced by the atmosphere, is a boundary layer for the interior quasigeostrophic motions. A boundary condition for the quasigeostrophic potential vorticity equation is obtained by matching the vertical velocities of the interior and boundary layer components just below the mixed layer. Using the mixed layer momentum Eq. (4b) and mixed layer vorticity Eq. (4e), the vertical velocity just below the mixed layer is

$$\hat{w}_+ = -\bar{h}\left(\frac{\partial \nabla^2 p}{\partial t} + \frac{\bar{R}o}{\delta}\bar{\boldsymbol{v}}\cdot\nabla\nabla^2 p + \frac{\hat{\beta}}{\delta}\frac{\partial p}{\partial x}\right)_{-\bar{h}}. \tag{5}$$

This vertical velocity $\hat{w}_+$ is matched to the interior vertical velocity which is determined from the interior equation for the conservation of buoyancy,

$$w = -\frac{1}{\gamma(z)}\frac{\partial^2 p}{\partial z \partial t}. \tag{6}$$

The matching condition at $z = -\lambda_m \bar{h}$ is,

$$\lambda_m \hat{w}_+ = w\left(-\lambda_m \bar{h}\right) \tag{7}$$

where $\lambda_m = \frac{\bar{H}}{D}$ and $\bar{H}$ is the previously defined depth scale for the mixed layer. The factor λ_m appears in front of $\hat{w}_+$ because $\hat{w}_+$ is scaled by $\bar{H}\omega Ro_1$, while w is scaled by $D\omega Ro_1$.

The quasigeostrophic potential vorticity Eq. (3) is easier to solve if the boundary condition is applied at the surface of the ocean ($z = 0$) instead of the base of the mixed layer ($z = -\lambda_m \bar{h}$). In order to extend the interior solution to $z = 0$, a solution is defined that satisfies Eq. (3) between the surface and the bottom of the mixed layer where $\gamma(z)$ varies continuously to $z = 0$. Since the boundary condition is on the vertical velocity, the vertical velocity must be extended to the surface. The vertical velocity can be Taylor expanded to about $z = 0$ because the mixed layer is shallow compared to the depth of the ocean (i.e., $\lambda_m \ll 1$)

$$w = w(0) + \frac{w(0) - \lambda_m \hat{w}_+}{\lambda_m \bar{h}} z + O\left(\lambda_m^2\right) \tag{8}$$

where the matching condition Eq. (6) has been used to determine the leading term in the expansion. From Eq. (3) and Eq. (6), it can be seen that

$$\frac{\partial \nabla^2 p}{\partial t} + \frac{\hat{\beta}}{\delta}\frac{\partial p}{\partial x} = \frac{\partial w}{\partial z}. \tag{9}$$

By substituting Eq. (5) and the vertical derivative of Eq. (8) into Eq. (9), the following equation for the vertical velocity at the surface is obtained:

$$w(0) = -\frac{\lambda_m \bar{R}o}{\delta}\bar{h}\bar{\boldsymbol{v}}\cdot\nabla\nabla^2 p|_0 \tag{10}$$

where terms of order λ_m^2 and higher have been neglected. Note that $w(0)$ represents the interior contribution to the surface vertical velocity; the sum of the interior and boundary

layer components vanishes in accordance with the rigid lid approximation. The vertical velocity $w(0)$ is a result of the divergence caused by the advection of the interior velocity by the Ekman velocity. This process does not depend on boundary layer structure; the same term would arise from a constant eddy viscosity boundary layer model. Finally, using Eq. (6) and Eq. (10) the surface boundary condition for the potential vorticity equation Eq. (3) is derived:

$$\frac{\partial^2 p}{\partial z \partial t} = \frac{\lambda_m \bar{R}o}{\delta} \gamma(0) \bar{h}\bar{v} \cdot \nabla \nabla^2 p \tag{11}$$

The boundary condition at the bottom of the ocean is $w = 0$ at $z = -1$, or using Eq. (6),

$$\frac{\partial^2 p}{\partial z \partial t} = 0. \tag{12}$$

As an example, the potential vorticity equation Eq. (3) with the boundary conditions Eq. (11) and Eq. (12) is solved for the special case of constant stratification ($\gamma(z) = S$). First, the quasigeostrophic pressure is separated as follows:

$$p(x,y,z,t) = \phi(z) e^{i(kx+ly-\sigma t)} \tag{13}$$

where k, i and σ are the nondimensional eastward wave number, northward wave number and frequency, respectively. Using Eq. (13), the potential vorticity equation Eq. (3) and the boundary conditions Eq. (11) and Eq. (12) become

$$\frac{d^2\phi}{dz^2} + \alpha^2 \phi = 0 \tag{14a}$$

$$\frac{d\phi}{dz} = -C\left[\alpha^2 + S(k^2 + l^2)\right]\phi \text{ at } z = 0 \tag{14b}$$

$$\frac{d\phi}{dz} = 0 \text{ at } z = -1 \tag{14c}$$

where

$$\alpha^2 = -S\left[(k^2 + l^2) + \frac{\hat{\beta}}{\delta}\frac{k}{\sigma}\right] \quad C = \frac{\lambda_m \bar{R}o}{\hat{\beta}} \frac{k^2 + l^2}{k} (k\tau^{(y)} - l\tau^{(x)})$$

and $\tau^{(x)}$ and $\tau^{(y)}$ are the nondimensional eastward and northward wind stress components. Eq. (2b) was used to relate the Ekman velocity to the wind stress.

The following eigenfunctions are solutions to Eq. (14a):

$$\phi_n = A_n \sin \alpha_n (z + 1) + B_n \cos \alpha_n (z + 1) \tag{15}$$

The bottom boundary condition Eq. (14c) is satisfied if $A_n = 0$. The surface boundary condition Eq. (14b) yields the following expression for the eigenvalues α_n:

$$\tan \alpha_n = \frac{C\left[\alpha_n^2 + S(k^2 + l^2)\right]}{\alpha_n} \tag{16}$$

In the MODE region, $\frac{\lambda_m \bar{R}o}{\hat{\beta}} \sim 6 \cdot 10^{-4}$, so C is very small and Eq. (16) can be solved approximately for small C. Assuming the zeroth eigenvalue to be very small (a nearly barotropic mode),

$$\alpha_0^2 \sim CS(k^2 + l^2) \tag{17}$$

The other eigenvalues are found by expanding in powers of C,

$$\alpha_n = \alpha_n^{(0)} + C\alpha_n^{(1)} + O(C^2) \tag{18}$$

Substituting Eq. (18) into Eq. (16) the eigenvalues are

$$\alpha_n^{(0)} = n\pi \tag{19a}$$

$$\alpha_n^{(1)} = n\pi + \frac{S(k^2 + l^2)}{n\pi} \tag{19b}$$

This expansion is valid for $Cn\pi < 1$.

Because the eigenvalues are real, the mixed layer does not cause the vertical structure function of the waves to damp or grow. The modal structures and frequencies are simply altered by a small amount. Thus in calculating the response of the mixed layer to perturbations by Rossby waves the Rossby wave modes can be calculated as if the mixed layer did not exist.

4.2. Surface mixed layer response to a rossby wave

The basic state mixed layer is driven by a constant wind stress and a constant positive surface buoyancy flux. Using Eq. (2c), the constant basic state mixed layer depth is

$$\bar{h} = \frac{2}{1 + \frac{2}{\hat{B}}} \tag{20}$$

and using Eq. (2a), the basic state buoyancy is

$$\bar{b} = \frac{t}{\bar{h}} \tag{21}$$

where the constant of integration has arbitrarily been chosen to be zero. Because the wind stress is spatially uniform there can be no wind stress curl contribution to the vertical velocity at the base of the mixed layer. However, if there is a zonal component of the wind there will be vertical velocity due to the advection of planetary vorticity. In this problem the basic state vertical velocity is ignored so that attention can be focused on the coupling between the Rossby wave and a basic state mixed layer in which the basic state ocean below the mixed layer is quiescent.

The basic state mixed layer is perturbed by a Rossby wave which is a solution to the linear quasigeostrophic potential vorticity equation Eq. (3) with boundary conditions $\frac{\partial^2 p}{\partial z \partial t} = 0$ at the surface and bottom of the ocean. The effect of the surface mixed layer on the Rossby wave was found to be small in Section 4.1; hence, the effect on the Rossby wave is ignored. The pressure field for a single Rossby wave at the bottom of the mixed layer is

$$p = \cos(kx + ly - t + \xi) \tag{22}$$

where k and l are the nondimensional eastward and northward wave numbers scaled by the horizontal wave number k_H and ξ is a phase constant. The Rossby wave dispersion relation is

$$1 + \lambda_r^2 = -\frac{\hat{\beta}}{\delta}k \tag{23}$$

Table 2
Vertical velocities at the bottom of the mixed layer for Rossby waves fit to the MODE data by McWilliams and Flierl (1976)

Wave	Period	Wavelength	Prop. dir.	α_r^2	$\frac{\bar{R}o}{\delta}(\bar{u}k + \bar{v}l)$
Barotropic #1	161	171	304	0	0.52
Barotropic #2	129	291	217	0	−0.35
Baroclinic #1	187	301	303	1.04	0.33
Baroclinic #2	332	290	208	0.96	−1.00

where $\lambda_r = \frac{L}{r}$ is the ratio of the horizontal length scale $L = k_H^{-1}$ and the Rossby radius r. In this problem, it is the vertical velocity at the bottom of the mixed layer caused by the Rossby wave that perturbs the mixed layer. Using Eq. (4b), Eq. (4e), Eq. (22) and Eq. (23), the vertical velocity at the base of the mixed layer is

$$\hat{w}_+ = A\bar{h}\sin(t - \theta) \tag{24}$$

where

$$A = \lambda_r^2 + \frac{\bar{R}o}{\delta}(\bar{u}k + \bar{v}l) \tag{25a}$$

$$\theta = kx + ly + \xi \tag{25b}$$

In this model, there are two mechanisms that produce vertical velocity at the bottom of the mixed layer represented by the two terms in Eq. (24) and Eq. (25a). The first term $\bar{h}\lambda_r^2\sin(t - \theta)$ is the vertical velocity at the mixed layer bottom due to vortex stretching by the Rossby wave that exists in the absence of the mixed layer. The second term $\frac{\bar{R}o}{\delta}\bar{h}(\bar{u}k + \bar{v}l)\sin(t - \theta)$ is the vertical velocity that arises from the divergence caused by the advection of the surface Rossby wave velocity by the Ekman velocity (or any other mean flow). Table 2 compares the two terms of the vertical velocity for the two barotropic and first two baroclinic Rossby waves that McWilliams and Flierl (1976) obtained from a wave fit to the MODE data. The vertical velocities in a barotropic Rossby wave are identically zero. Therefore, with a barotropic Rossby wave the vertical velocity at the base of the mixed layer results only from the second mechanism. There are vertical velocities in a baroclinic Rossby wave and in Table 2 it can be seen that the vertical velocities at the base of the mixed layer resulting from the two mechanisms are comparable. Thus, even though the vertical velocity arising from the second mechanism does not affect the Rossby waves, it is as important as the vertical velocity of the Rossby wave in perturbing the mixed layer.

The mixed layer depth response to a Rossby wave is found by solving the turbulent kinetic energy equation Eq. (4c), the entrainment equation Eq. (4d) and the equation for buoyancy below the mixed layer Eq. (4f). The response is calculated first during detrainment and second during entrainment. The method, which is similar to that used by Gill and Turner (1976), is first discussed and then the solution itself will be presented.

During detrainment the mixed layer depth and buoyancy are easily found from the turbulent kinetic energy Eq. (4c) and buoyancy Eq. (4a) equations. The buoyancy jump

at the bottom of thee mixed layer is zero during detrainment. Hence, from Eq. (4c) the perturbation mixed layer depth $\hat{h}$ is zero. Eq. (4a) becomes

$$\frac{\partial \hat{b}}{\partial t} + \frac{\overline{Ro}}{\delta}\bar{\boldsymbol{v}} \cdot \nabla \hat{b} = 0 \tag{26}$$

Thus, moving with the Ekman flow the perturbation buoyancy $\hat{b}$ is constant throughout the period of detrainment.

In order to calculate the perturbation buoyancy below the mixed layer $\hat{b}_r$ the advection of the buoyancy $\hat{b}_r$ by the basic state velocity below the mixed layer $\left(\frac{\overline{Ro}}{\delta}\bar{\boldsymbol{v}} \cdot \nabla \hat{b}_r\right)$ is neglected.The reason for ignoring this term is that it is not obvious how the find the basic state velocity below the mixed layer. Below the mixed layer the basic state velocity is no longer balanced by the wind stress; therefore, it must undergo geostrophic adjustment. The relative importance of buoyancy advection by this velocity is not known.

To find the buoyancy below the mixed layer let h_m be the distance from a fluid parcel of a given buoyancy to the bottom of the mixed layer. Using Eq. (24), the equation for buoyancy below the mixed layer Eq. (4f) is replaced by

$$-\frac{\partial h_m}{\partial t} = A\bar{h}\sin(t-\theta) \tag{27}$$

Eq. (27) is a statement that only the vertical motion of the fluid parcels below the mixed layer is important. Upon integrating Eq. (27), h_m is found to be

$$h_m = A\bar{h}(\cos(t-\theta) - \cos(t'-\theta)) \tag{28}$$

where h_m is the distance from the bottom of the mixed layer to the fluid parcel of buoyancy $b(t')$ and t' is the time when that fluid parcel was detrained.

From the entrainment equation Eq. (4d), it can be seen that during detrainment the vertical velocity $\hat{w}_+$ must be negative since $\hat{h}$ is zero. Inspection of Eq. (24) reveals that for $A > 0$ $\hat{w}_+$ is negative for $\theta - \pi < t < \theta$. However, detrainment does not necessarily start at $t = \theta - \pi$ because if the mixed layer is deepening faster than the downward movement of the fluid just below the mixed layer (i.e., $\frac{\partial \hat{h}}{\partial t} > -\hat{w}_+$) then entrainment is occurring. Thus, at some time after $\theta - \pi$, which cannot be determined a priori, detrainment starts. Detrainment ends and entrainment begins when the fluid just below the mixed layer stops moving down and begins to move up (i.e., when $\hat{w}_- = 0$). This occurs at $t = \theta$.

During entrainment the perturbation mixed layer depth varies. The equation for the distance between the fluid parcel of buoyancy $b(t')$ and the bottom of the mixed layer is

$$-\frac{\partial h_m}{\partial t} = \frac{\partial \hat{h}}{\partial t} + A\bar{h}\sin(t-\theta) \tag{29}$$

Upon integration h_m is

$$h_m = -\hat{h} + A\bar{h}(\cos(t-\theta) - \cos(t'-\theta)) \tag{30}$$

where the constant of integration has been chosen so that h_m is continuous at $t = \theta$. A time τ_h can defined as the time during detrainment when the mixed layer buoyancy $b(\tau_h)$ equals the buoyancy $b_+(t)$ just below the mixed layer at time t during entrain-

ment. When $t' = \tau_h$ the fluid of buoyancy $b(t')$ is at the bottom of the mixed layer (i.e., $h_m = 0$). Using this information in Eq. (30) yields an expression for the perturbation depth

$$\hat{h} = A\bar{h}(\cos(t-\theta) - \cos(\tau_h - \theta)) \tag{31}$$

The equation relating t and τ_h is found from the turbulent kinetic energy equation Eq. (4c). First, the total buoyancy jump must be related to t and τ_h. From the definition of τ_h and Eq. (21)

$$\begin{aligned}
&\left(\bar{b} - \bar{b}_+\right) + \left(\hat{b} - \hat{b}_+\right) = b(t) - b_+(t) \\
&= b(t) - b(\tau_h) \\
&= \frac{1}{\bar{h}}(t - \tau_h) + O(Ro_l)
\end{aligned} \tag{32}$$

Using Eqs. (4c) and (4d), Eq. (31) and Eq. (32), the equation relating t and τ_h is

$$\frac{d\tau_h}{dt} = \frac{\left(1 + \frac{2}{\hat{B}}\right)(\cos(t-\theta) - \cos(\tau_h - \theta))}{(\tau_h - t)\sin(\tau_h - \theta)} \tag{33}$$

where it is again assumed that the perturbation velocity below the mixed layer is negligible. The phase θ can be eliminated by the following change of variables

$$\begin{aligned}
t^* &= t - \theta \\
\tau_h^* &= \tau_h - \theta
\end{aligned} \tag{34}$$

Hence,

$$\frac{d\tau_h^*}{dt^*} = \left(1 + \frac{2}{\hat{B}}\right)\frac{\cos t^* - \cos\tau_h^*}{(\tau_h^* - t^*)\sin\tau_h^*} \tag{35}$$

where it is assumed that τ_h^* is a function of $t - \theta$ only. Eq. (35) is numerically integrated using a second order Runge–Kutta algorithm (Press et al., 1986) with the initial condition $\tau_h^* = 0$ at $t^* = 0$. Entrainment ceases at $t^* - \tau_h^* = 2\pi$, when the first fluid parcel that left the mixed layer during detrainment is entrained back into the mixed layer. Thus, the time when detrainment starts is determined. The perturbation mixed layer depth is given by Eq. (31). The perturbation mixed layer buoyancy is obtained from the buoyancy equation Eq. (4a), which, together with Eq. (2a) and Eq. (4c), becomes

$$\bar{h}\frac{\partial \hat{b}}{\partial t} + \frac{\bar{R}o}{\delta}\bar{h}\bar{v}\cdot\nabla\hat{b} = \frac{2}{\hat{B}}\frac{\hat{h}}{\bar{h}} \tag{36}$$

The perturbation buoyancy and mixed layer depth for the special case $\bar{R}_o \ll \delta$ are shown as functions of time t^* for one Rossby wave period in Fig. 1 and Fig. 2. In Fig. 3, profiles of buoyancy are shown for various times during the Rossby wave period. The three figures show that there is a growing buoyancy jump that moves up and down sinusoidally with motion of the Rossby wave. During detrainment the mixed layer stays at a constant depth $\bar{h}$ while the buoyancy jump moves down. As the buoyancy in the mixed layer increases due to the positive surface buoyancy flux, fluid leaves the bottom

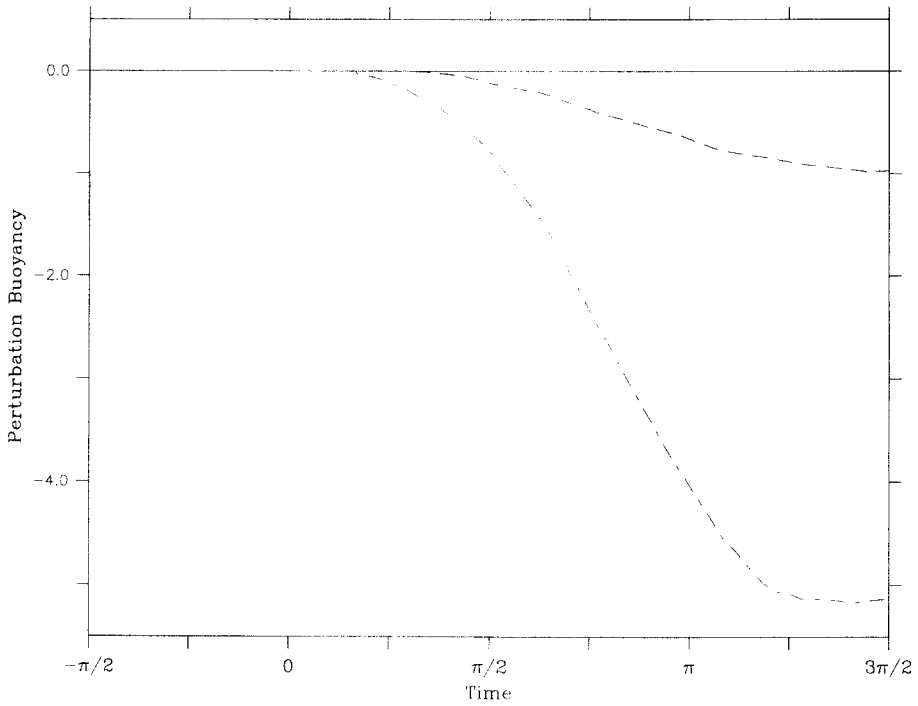

Fig. 1. Perturbation buoyancy as a function of time for $\bar{R}_{,} \ll \delta$ and $\hat{B} = \infty$ (solid line), $\hat{B} = 1$ (dashed line), and $\hat{B} = 4$ (dashed–dotted line).

of the mixed layer resulting in a stratified region between the bottom of the mixed layer and the buoyancy jump. Entrainment starts at $t^* = 0$ when the buoyancy jump starts to move back up. The water that left the mixed layer during detrainment re-enters the mixed layer during entrainment. As entrainment proceeds a smaller buoyancy jump builds up at the bottom of the mixed layer because the mixed layer buoyancy increases from the time a water parcel leaves the mixed layer during detrainment to the time it re-enters during entrainment. As is evident from the turbulent kinetic energy equation Eq. (4c) during entrainment the mixed layer becomes shallower. The reason for this is that some of the turbulent kinetic energy is used to mix the entrained water thus leaving less turbulent kinetic energy to mix the buoyancy added at the surface. Entrainment continues as the large buoyancy jump begins to move back down; that is, the mixed layer deepens more rapidly than the water below. Just as the mixed layer deepens back to the depth $\bar{h}$, it entrains the last of the water between the mixed layer and the large buoyancy jump. Thus, the buoyancy jump at the bottom of the mixed layer adds to the large buoyancy jump. This completes the cycle and detrainment once again begins.

During entrainment for finite $\hat{B}$ the perturbation buoyancy decreases. Meanwhile, the basic state buoyancy is increasing due to the surface buoyancy flux. Hence, the effect of the Rossby wave is to lower the rate of increase of mixed layer buoyancy at a fixed point in space. There is also spatial structure in the buoyancy response to the Rossby wave as shown in Fig. 1 (remember, $t^* = t - \theta$). The buoyancy increases in the

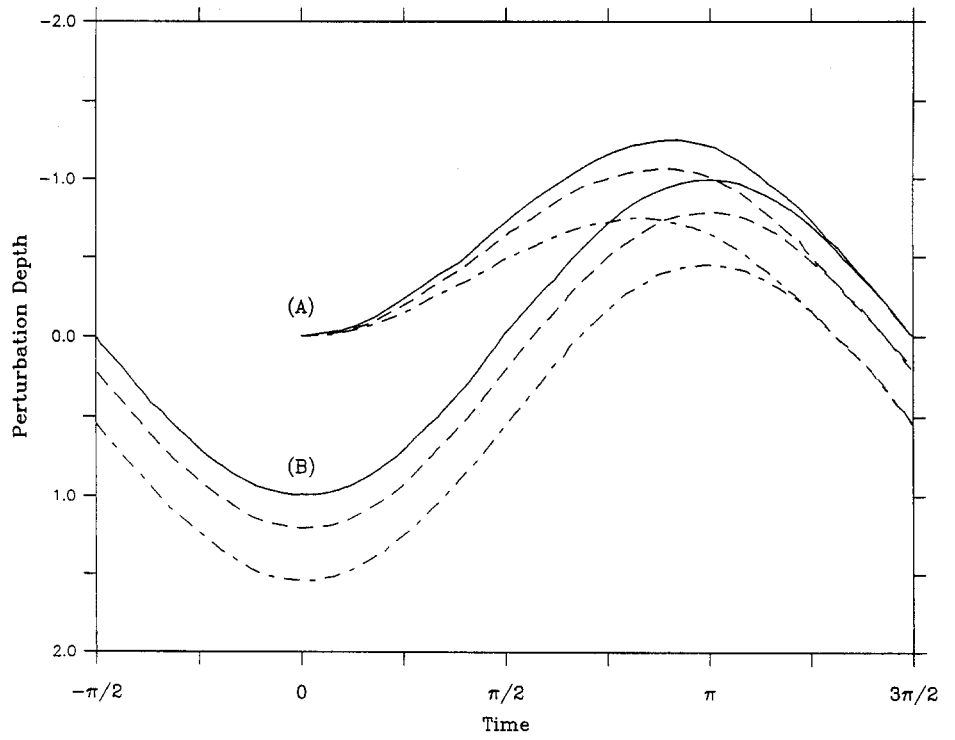

Fig. 2. (a) Perturbation depth, and (b) location of the large buoyancy jump relative to the bottom of the mixed layer as functions of time for $\overline{R}_o \ll \delta$ and $\hat{B} = \infty$ (solid line), $\hat{B} = 1$ (dashed line), and $\hat{B} = 4$ (dashed–dotted line).

direction that the Rossby wave propagates. For $\hat{B} = \infty$ (i.e., there is no dissipation) the Rossby wave does not affect the mixed layer buoyancy.

The reason that the perturbation buoyancy decreases for finite $\hat{B}$ and is zero for $\hat{B} = \infty$ is as follows. For finite $\hat{B}$, the Rossby wave causes more water to be in contact with the surface as the average depth of the large buoyancy jump is greater than $\overline{h}$. On the other hand, for $\hat{B} = \infty$ the average depth of the large buoyancy jump is equal to $\overline{h}$. In the presence of the Rossby wave the mixed layer is shallower than $\overline{h}$ during detrainment. Hence, for finite $\hat{B}$ there is less dissipation of turbulent kinetic energy than in the absence of the Rossby wave. With less dissipation, there is more turbulent kinetic energy available to mix the buoyancy added at the surface throughout a greater volume of water. Therefore, the buoyancy increases less rapidly in the presence of the Rossby wave. In the case when $\hat{B} = \infty$, there is no background dissipation so the same amount of turbulent kinetic energy is available for mixing whether the wave is present or not.

The Ekman velocity advects the perturbation buoyancy that arises for finite $\hat{B}$. To calculate the effect of this advective flux equation Eq. (36) can be rewritten as follows

$$\frac{\partial \hat{b}}{\partial t} + \frac{\overline{Ro}}{\delta}(\overline{u}k + \overline{v}l)\frac{\partial \hat{b}}{\partial \theta} = \frac{2\hat{h}}{\hat{B}\overline{h}^2} \tag{37}$$

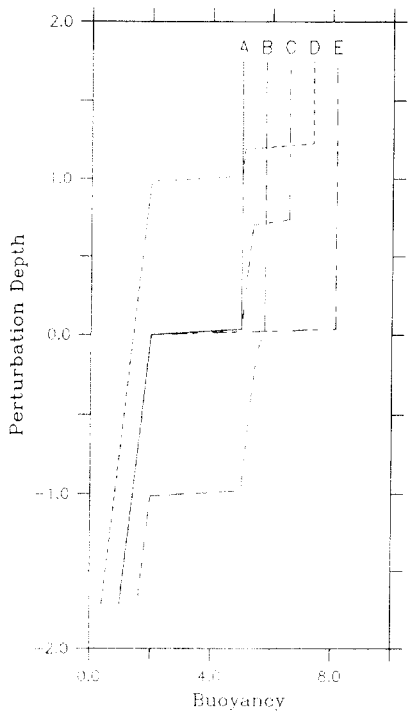

Fig. 3. Profiles of buoyancy for $\hat{B} = \infty$ at times (a) $-\frac{\pi}{2}$, (b) 0, (c) $\frac{\pi}{2}$, (d) π, (e) $\frac{3\pi}{2}$.

as the advection occurs only in the propagation direction of the wave. Furthermore, since the perturbation buoyancy is a function of $t - \theta$ only Eq. (37) can be rewritten using Eq. (31)

$$\left(1 - \frac{\bar{R}o}{\delta}(\bar{u}k + \bar{v}l)\right)\frac{\partial \hat{b}}{\partial t^*} = \frac{2A}{\hat{B}\hat{h}}(\cos t^* - \cos\tau_h^*) \tag{38}$$

Thus, when advection is important the perturbation buoyancy is found by integrating Eq. (38).The extra factor $\left(1 - \frac{Ro}{\delta}(\bar{u}k + \bar{v}l)\right)$ is greater than one if the Ekman velocity has a component in the direction opposite to which the Rossby wave is propagating. In this case, the buoyancy decreases slower as t^* increases because the Ekman velocity advects in greater values of $\hat{b}$. On the other hand, the factor is positive and less than one if the Ekman velocity has a component in the direction the wave is propagating and this component is less than the phase speed of the wave. In this case, buoyancy decreases faster as t^* increases because the Ekman velocity advects in smaller values of $\hat{b}$. The factor is negative if the Ekman velocity has a component in the direction the Rossby wave is propagating and this component is greater than the phase speed. In this case, the buoyancy increases with increasing t^*. The reason is as follows. When the mixed layer fluid moves past the Rossby wave in a frame of reference fixed to the moving wave its buoyancy decreases. With no Ekman velocity the fluid moves eastward relative to the wave. Hence, $\hat{b}$ decreases to the west and increases as t^* increases.

5. Numerical simulations

5.1. The numerical model

The surface mixed layer response to the Rossby wave described in Section 4.2 was used as a comprehensive test problem for a numerical model of boundary layer interactions with the ocean interior. The coupled quasigeostrophic–surface boundary layer (QGSBL) model described by Walstad and Robinson (1993) is formulated to represent the same basic physics as the preceding, but is not strictly limited to linear problems. The prognostic vorticity equation is

$$\frac{\partial \zeta}{\partial t} + \alpha J(\psi,\zeta) + \beta\psi_x = F_{pqr}$$

where

$$\zeta = \nabla_H^2\psi + \Gamma^2(\sigma\psi_z)_z$$

and the Jacobian $J(\psi,\zeta) = \psi_x\zeta_y - \psi_y\zeta_x$. The nondimensional parameters are

$$\alpha = \frac{V_0 t_0}{D}$$

$$\beta = \beta_0 D t_0$$

$$\Gamma^2 = \frac{f_0^2 D^2}{N_0^2 H^2}$$

where

$$f_0 = 2\Omega\sin\Theta_0$$

$$\beta_0 = \frac{\partial f}{\partial y}$$

and D, H, t_0 and V_0 are characteristic length, depth, time and velocity scales. The stratification is given by

$$\sigma(z) = \frac{N_0^2}{N^2}$$

where

$$N^2 = -\frac{g}{\rho}\frac{\partial \rho}{\partial z}$$

The surface and bottom boundary conditions provide prognostic equations for the top and bottom density

$$\frac{\partial \Gamma^2\sigma\psi_z}{\partial t} + \alpha J\left(\psi,\Gamma^2\sigma\psi_z\right) = \begin{cases} w^1 & \text{at z} = 0 \\ -\kappa\nabla_H^2\psi - J(\psi,b) & \text{at z} = -\text{Z} \end{cases}$$

where κ is the bottom friction applied over the topography b. The dimensional quasigeostrophic vertical velocity $w^{QG} = \frac{V_0 H}{f_0 t_0 D} w^1$ is balanced by the Ekman vertical velocity to maintain the rigid lid approximation at the sea surface

$$w^{QG} + w^E = 0 \text{ at } z = 0$$

The horizontal Ekman velocities are given by

$$\mu = \frac{\partial}{\partial z}\left(\frac{\hat{j}\cdot\vec{\tau}}{\rho}\right) \quad \nu = -\frac{\partial}{\partial z}\left(\frac{\hat{i}\cdot\vec{\tau}}{\rho}\right)$$

with transports

$$\mu_T = \frac{\hat{j}\cdot\vec{\tau}}{\rho_0 f_0} \quad \nu_T = -\frac{\hat{i}\cdot\vec{\tau}}{\rho_0 f_0}$$

The quasigeostrophic contribution to the total vertical velocity at the surface is

$$w^{QG}(z=0) = \frac{\partial \mu_T}{\partial x} + \frac{\partial \nu_T}{\partial y} - \frac{1}{f_0}(\mu_T R_x + \nu_T R_y) - \frac{\beta_0}{f_0}\nu_T$$

where R is the relative vorticity at the surface

$$R = \frac{V_0}{D}\nabla_H^2 \psi|_{z=0}$$

Vertical velocities are assumed to vary linearly with depth in this model. As the boundary condition sets the surface value, the vertical derivative of the vertical velocity is used to interpolate

$$w_z^{QG} = -\frac{V_0 \Gamma^2}{f_0 t_0 D}\frac{D}{Dt}(\sigma\psi_z)_z$$

The surface boundary layer component of the vertical velocity ω is assumed to vanish at the base of the mixing layer, so it varies linearly between $-w^{QG}$ and 0 between $z=0$ and $z=-h$. Equations for the boundary layer buoyancy and temperature evolution are

$$\rho_t + \alpha\left(J(\psi^*,\rho) + \mu(\delta_x^* + \rho_x) + \nu(\delta_y^* + \rho_y) + (w^{QG}+\omega)\rho_z\right) - \frac{\omega}{\Gamma^2\sigma} = (M_\rho)_z + \frac{\alpha_T}{\rho_0 c_P} I_z$$

$$\vartheta_t + \alpha\left(J(\psi^*,\vartheta) + \mu(\delta_x^* + \vartheta_x) + \nu(\delta_y^* + \vartheta_y) + (w^{QG}+\omega)\vartheta_z\right) - \omega\Theta_z = (M_\vartheta)_z + \frac{1}{\rho_0 c_P} I_z$$

where $(M\rho)z$ and $(M\theta)z$ represent mixing terms which are composed of instantaneous homogenization within the mixed layer and constant diffusion below. The final terms on the right hand sides represent the divergence of the penetrative surface heat flux (short wave solar radiation). In these equations, the quasigeostrophic streamfunction dimensionalized according to

$$\psi^* = V_0 D\psi.$$

The density and temperature perturbations to the mean stratification due to interior motions are

$$\delta^* = \frac{\rho_0 f_0 V_0 D}{gH\sigma}(\sigma\psi_z)|_{z=0}$$

$$\theta = \frac{V_0 H \Gamma^2}{f_0 D} \Theta_z (\sigma \psi_z)|_{z=0}$$

where Θ represents the mean vertical temperature gradient. The mixing layer depth equation is

$$h_t + uh_x + vh_y + w = e$$

where the entrainment rate e is the flux across the base of the mixing layer. This quantity is normally derived from the Garwood (1977) entrainment model. To facilitate quantitative comparisons between the numerical and analytic solutions this module of the algorithm was replaced with a representation of the turbulent kinetic energy budget given in Eq. (4c).

5.2. Results

The first comparison of the numerical results from the QGSBL model with the semianalytic solution revealed a number of significant discrepancies between the two. The problems resulted from a failure to maintain the fidelity of the discontinuity in properties between the bulk mixed layer and the remnant layer below. Nearly all of the horizontal, vertical and temporal operators in the boundary layer model computed differences across the base of the mixed layer, resulting in unphysical leakage of material between the two layers. The troublesome algorithms were redesigned to insure that the only transfer of properties across the mixing layer depth interface is that prescribed by the entrainment function. These modifications will now be described. [3]

First, the vertical advection algorithm was changed from the second order uncentered method described in Walstad and Robinson (1993) to a modified first order upwind differencing scheme. Upwind techniques are known to be effective in applications in which the advected quantity undergoes sudden changes of state (Press et al., 1986). In the present problem, it is the discontinuity between the mixing and remnant layers that must be preserved. No material must pass through the interface between the two layers except that which is prescribed by the entrainment equation. In the old vertical advection scheme, the finite differences were computed across the mixing layer interface resulting in substantial exchange between the two layers. Leakage of this type is eliminated in the modified upwind technique.

For a scalar ϕ, the difference equations are

$$(\phi_z)_k = c_{-1}\phi_{k-1} + c_0\phi_k + c_1\phi_{k+1}$$

$$c_0 = -(c_{-1} + c_{+1})$$

For $w_k \leq 0$ and $k \neq k_{ml} + 1$ (where k_{ml} represents the grid point whose model level depth is the deepest of all those in the mixing layer),

$$c_{-1} = \frac{1}{z_{k-1} - z_k}$$

[3] The following algorithmic improvements overcome the computationally cumbersome problem of coupling a bulk boundary layer to an interior model configured on level surfaces. An alternative approach would be to reformulate the boundary layer model in a level-by-level discretization.

and

$$c_{-1} = 0.$$

When $w_k \leq 0$ and $k = k_{ml} + 1$, care must be taken in order not to advect material across the mixing layer depth interface. The desired finite difference is that between layer k and the point just below the mixing layer. But, the point just below the mixing layer resides in layer k, so there is no gradient because of the 'layer' model discretization. Therefore, in this case $c_{-1} = c_{+1} = 0$. For $w_k > 0$ and $k \neq k_{ml}$,

$$c_{+1} = \frac{1}{z_{k+1} - z_k}$$

and

$$c_{-1} = 0$$

Again, when $w_k > 0$ and $k = k_{ml}$, $c_{-1} = c_{+1} = 0$ to prevent leakage across the mixing layer depth interface. Boundary conditions must be specified at the bottom and top of the SBL grid during upwelling and downwelling, respectively. When $w_k \leq 0$ and $k = 1$, $c_{-1} = c_{+1} = 0$ as the gradient is assumed to vanish at the surface. When $w_k > 0$ and $k = l$, a boundary value ϕ_l must be prescribed.

The second change to the model was necessary to maintain the fidelity of the two layers during horizontal advection and filtering operations. In the presence of a spatially varying mixing layer depth field, simple horizontal operators will compute differences across the interface between the mixing and remnant layers. In order to remedy this problem, two level surfaces are defined at each time step that bound the upper and lower excursions of the mixing layer depth field. Above and below these surfaces the relevant fluxes are computed in the normal fashion using the appropriate operator (the Arakawa Jacobian for advection and the Shapiro filter for dissipation). Between these surfaces things are a little more complicated. At each vertical level, a surface is defined that is as close to the horizontal as possible but follows the interface contour when necessary to prevent crossing it. Scalar values from these deformed surfaces are then sent to the appropriate operator to compute the fluxes. This technique is illustrated in Fig. 4. Consider the two dimensional x–z grid shown. The mixing layer depth in each column is indicated by an asterisk, and the interface between the mixing and remnant layers is approximated by the bold solid line connecting those points. Because the excursions of the interface do not reach rows 1 or 4, horizontal advections are computed there using the normal procedure. Now, for each of the rows in the interfacial region, both mixing layer and remnant layer advection terms must be computed. In the figure, the stretched surfaces on which the Jacobian operates are indicated by dashed and long-dashed lines for rows 2 and 3, respectively. After remnant and mixing layer advections terms have been computed for each point in the interfacial region, the algorithm selects which term to incorporate at each point according to its position relative to the interface.

Just as the fidelity of the mixing layer depth interface must be maintained in the spatial differencing, it must also be carefully treated in the temporal dimension. Consider the methods by which the various terms are time stepped. The 'mixing' terms (all those in the buoyancy equation except for the advection terms) are marched ahead in time using a simple forward Eulerian technique, while the advective terms are time stepped using a leapfrog method. Implementation of this approach requires that two

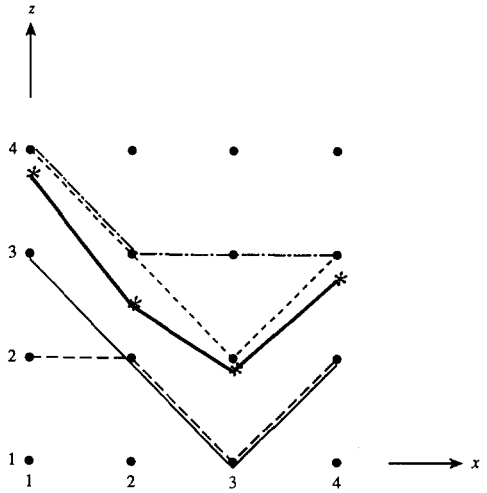

Fig. 4. A schematic diagram of the method used to deform surfaces in the transition layer for subsequent horizontal numerical operations.

solutions be maintained during an integration, one representing the model state at time t and one in which the advective terms lag by one time step δt. The advection terms are moved forward in time in a fashion schematized in Fig. 5. The advective terms are computed from solution II, multiplied by $2\delta t$ and added to solution I, yielding solution III that now leads solution II by δt in the advective terms only. At this point, the mixing terms are computed for both solutions and advanced δt. This results in an analogous configuration to that with which the cycle was begun; we have a physical solution at time $t + \delta t$ and a solution that lags by δt in the advective terms only.

Unphysical transport of properties across the mixed layer depth interface can result if the implementation of this leapfrog time stepping procedure is not carefully treated. This results from the fact that the mixed layer–remnant layer grid configuration changes over time. That is, a given gridpoint that is in the mixed layer in solution II (Fig. 5) does not necessarily reside in the mixed layer in solution I, to which the advective terms computed from solution II are added. This situation is remedied by mapping the advective terms from solution II to solution I in the two regimes (mixed layer and remnant layer) separately. The mapping technique is illustrated in Fig. 6. This approach

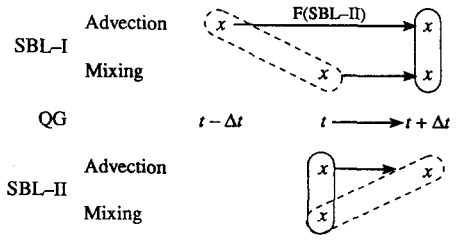

Fig. 5. A schematic diagram of the time stepping procedure used in the surface boundary layer model.

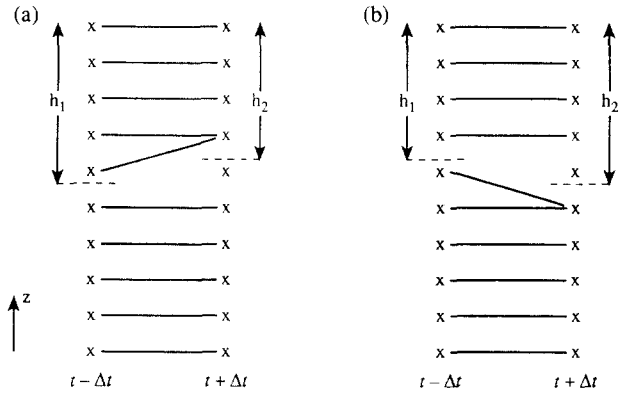

Fig. 6. A schematic diagram of the mapping used for the time stepping of advection terms for the case in which the mixed layer grid in solution II is (a) shallower than solution I, and (b) deeper than solution I.

insures that mixed layer advective fluxes remain in the mixed layer and remnant layer fluxes remain in the remnant layer.

With these improvements in place, the numerical model accurately represents the semi-analytic solution of the mixed layer response to a Rossby wave. Fig. 7 shows a time series of maps of streamfunction, vorticity, vertical velocity, mixing layer depth, and the normalized root mean square difference between the mixing layer depth field of the numerical and semianalytic solutions for approximately 1 wave period. Fig. 8 shows that the spatially averaged normalized root mean square error in mixing layer depth is well within acceptable limits, as the average error does not exceed 8%. The marked periodicity of the error trajectory is due to the fact that the model domain is not large enough to contain a full wavelength of the Rossby wave. The important points here are that (1) the maximum error never gets too large, and (2) the average error (which is more representative of an integrated error value) is comparable to the error levels present in the interior quasigeostrophic model (Robinson and Walstad, 1987). Here, it must be noted that the size of the domain used in such a comparison does in fact influence the integrated error because perfect information is being fed into the domain at inflow points. A greater percentage of the area of a smaller domain will be influenced by this inflow of information, thus, artificially improving the error estimate.

Analysis of a time series of the buoyancy profile for the center point in the model domain shows excellent agreement throughout the simulation (Fig. 9). In the initial condition, the vertical velocity at the center of the domain has just changed sign. Thus, the period of detrainment has just concluded, and entrainment is about to begin. This situation is analogous to profile B in Fig. 3. In this panel, the numerical solution (solid line) and the semianalytic solution (dashed line) are coincident. Throughout the period of entrainment($t = 20,40,60$) and subsequent detrainment ($t = 80$, 100), the numerical solution tracks the semianalytic solution extremely well. The only discrepancy between the two profiles is in the region of the buoyancy jump in the remnant layer. The numerical solution does not maintain the sharp gradient of the analytic solution in the remnant layer only. This is attributable to the numerical diffusion, or artificial viscosity

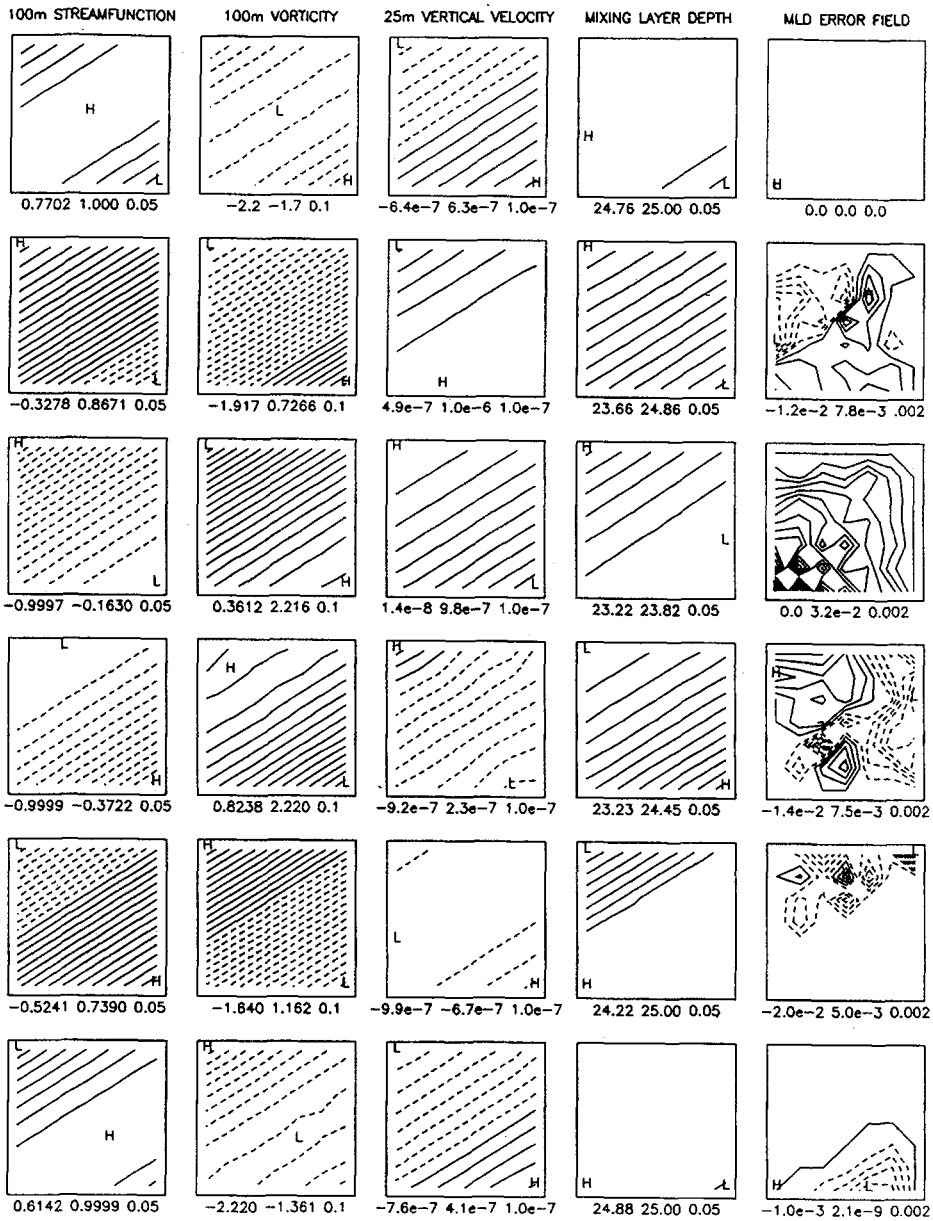

Fig. 7. A time series of streamfunction at 100 m, vorticity at 100 m, vertical velocity at 25 m, mixing layer depth and mixing layer depth error (normalized root mean square) fields for (a) $t = 0$, (b) $t = 20$, (c) $t = 40$, (d) $t = 60$, (e) $t = 80$, (f) $t = 100$ days.

inherent in the vertical differencing scheme employed in the numerical model (Roache, 1972), but not included in the semianalytic solution. The magnitude of the artificial viscosity is controlled by computational parameters (the grid interval and the time step).

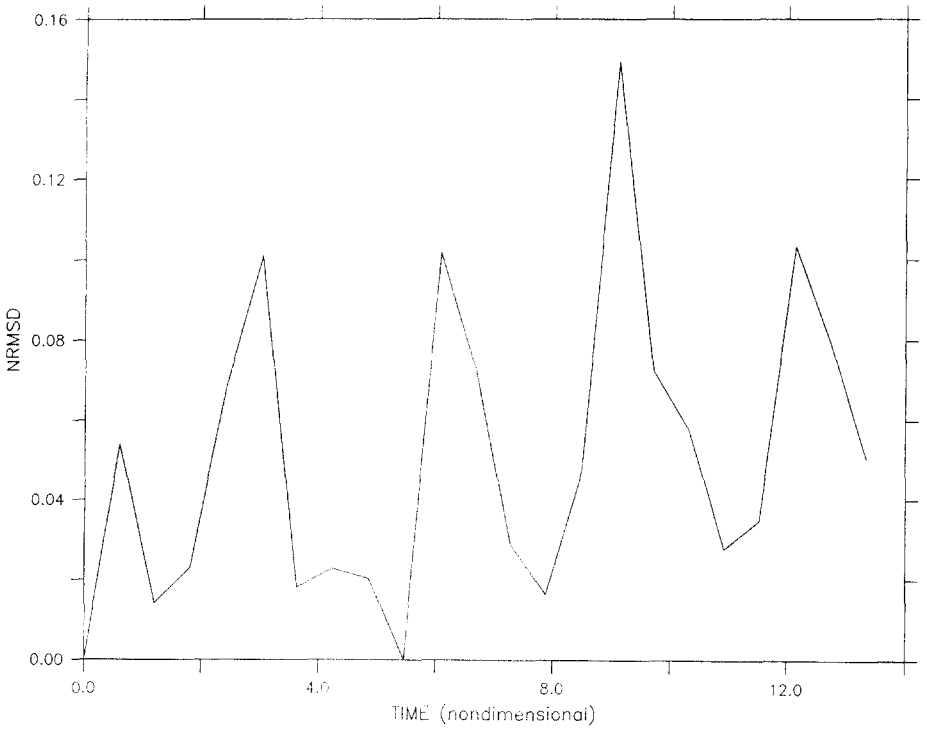

Fig. 8. A time series of the integrated normalized root mean square error of the mixing layer depth field.

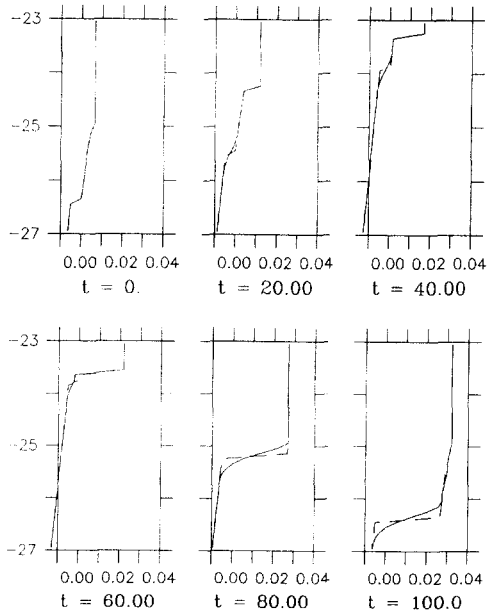

Fig. 9. A time series of vertical profiles of buoyancy for the numerical solution (solid line) and the semianalytic solution (dashed line).

For the present case the artificial viscosity is more than an order of magnitude less than the commonly accepted value for physical diffusion in the remnant layer of the real ocean (1 cm^2/s). Because the intent here is to construct a model capable of simulating the real ocean, this error source is of no concern as it will be swamped by physical diffusive processes.

6. Conclusions

A detailed description of the interaction between a Rossby wave and a surface mixed layer has been presented. It is demonstrated that the presence of the mixed layer has negligible impact of the wave itself. However, the vertical motions induced by vortex stretching in the interior and the divergence caused by the advection of the interior velocity by the wind driven flow dramatically affect the evolution of the boundary layer structure. Alternating periods of upwelling and downwelling not only move the mixed layer up and down, but also cause entrainment and detrainment. This results in the production of complex remnant layer structures during some parts of the wave period. The magnitude of the boundary layer disturbance caused by the interaction is fundamentally controlled by the strength of the Ekman flow and the amplitude of the Rossby wave. This idealized problem has been used to benchmark a coupled quasigeostrophic and surface boundary layer model. Intricate numerical techniques are required to prevent unphysical flux of material through the mixing layer depth interface when the depth of this interface varies in space and time.

Acknowledgements

D.J.M. and A.R.R. gratefully acknowledge the Office of Naval Research grants N00014-90-J-1593 and N00014-95-1-0371. D.J.M. was also supported by the Office of Naval Research Graduate Fellowship and subsequently by a UCAR Postdoctoral Modelling Fellowship with a simultaneous WHOI Postdoctoral Scholarship. We would also like to thank Dr. Leonard Walstad for the many stimulating discussions about the physics of the upper ocean and the numerics of the coupled model. Woods Hole Oceanographic Institution Contribution 9330.

References

Garwood, R.W., 1977. An oceanic mixed layer model capable of simulating cyclic states. J. Phys. Ocean. 7, 455–468.

Gill, A.E., Turner, J.S., 1976. A comparison of seasonal thermocline models with observations. Deep Sea Res. 23, 391–401.

Klein, P., Hua, B.L., 1988. Mesoscale heterogeneity of the wind-driven mixed layer: Influence of a quasigeostrophic flow. J. Mar. Res. 46, 495–525.

Kunze, E., 1985. Near-inertial wave propagation in geostrophic shear. J. Phys. Ocean. 15, 544–656.

Lee, D.K., Niiler, P., Warn-Varnas, A., Piacsek, S., 1994. Wind-driven secondary circulation in ocean mesoscale. J. Mar. Res. 520, 371–396.

Martin, P.J., 1985. Simulation of the mixed layer at OWS November and Papa with several models. J. Geophys. Res. 90, 903–916.

McGillicuddy, D.J., Robinson, A.R., 1997. Eddy Induced Nutrient Supply and New Production in the Sargasso Sea. in press, Deep Sea Res.

McGillicuddy, D.J., Robinson, A.R., McCarthy, J.J., 1995. Coupled physical and biological modelling of the spring bloom in the North Atlantic: II. Three dimensional bloom and post-bloom effects. Deep Sea Res. 42, 1359–1398.

McWilliams, J.C., Flierl, G.R., 1976. Optimal quasigeostrophic wave analysis of MODE array data. Deep Sea Res. 23, 285–300.

Niiler, P.P., 1969. On the Ekman divergence in an oceanic jet. J. Geophys. Res. 74, 7048–7052.

Press, W.H., Flannery, B.P., Teukolsky, S.A., Vetterling, W.T., 1986. Numerical Recipes. Cambridge Univ. Press, Cambridge.

Price, J.F., Terray, E.A., Weller, R.A., 1987. Upper ocean dynamics. Rev. Geophys. 25, 193–203.

Roache, P., 1972. Comput. Fluid Dynamics. Hermosa Publishing, Albuquerque.

Robinson, A.R., 1983. Eddies in Marine Sci. Springer-Verlag, New York.

Robinson, A.R., Walstad, L.J., 1987. The Harvard open ocean model: Calibration and application to dynamical process, forecasting, and data assimilation studies. Appl. Num. Math. 3 (1–2), 89–131.

Stern, M.E., 1965. Interaction of a uniform wind stress with a geostrophic vortex. Deep Sea Research 12, 355–367.

Stevenson, J.W., 1980. Response of the surface mixed layer to quasigeostrophic oceanic motions. Ph.D. thesis, Harvard Univ., Cambridge, MA 02138.

Stevenson, J.W., 1983. The seasonal variation of the surface mixed layer response to the vertical motions of linear Rossby waves. J. Phys. Ocean. 13, 1255–1268.

Walstad, L.J., Robinson, A.R., 1993. A coupled surface boundary layer–quasigeostrophic model. Dyn. Atmos. Oceans 18, 151–207.

Weller, R.A., 1982. The relation of near-inertial motions observed in the mixed layer during the JASIN (1978) experiment to the local wind stress and to the quasigeostrophic flow field. J. Phys. Ocean. 12, 1122–1136.

Weller, R.A., 1985. Near surface velocity variability at inertial and subinertial frequencies in the vicinity of the California current. J. Phys. Ocean. 15, 372–385.